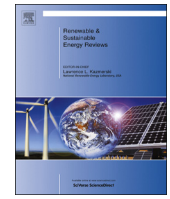
Renewable and Sustainable Energy Reviews 26 (2013) 408–413

Contents lists available at SciVerse ScienceDirect

Renewable and Sustainable Energy Reviews

journal homepage: www.elsevier.com/locate/rser



Simulation of photogenerated current of PN silicon photodetector enhanced by impurity photovoltaic effect

Wagah F. Mohammed [a,*], Mudhar A. Humoody [a], Munther N. Al-Tikriti [b]

[a] *College of Engineering, Mosul University, Mosul, Iraq*
[b] *Faculty of Engineering, Philadelphia University, Amman, Jordan*

ARTICLE INFO

Article history:
Received 9 February 2013
Received in revised form
21 May 2013
Accepted 26 May 2013
Available online 29 June 2013

Keywords:
Silicon photodetectors
Photogenerated current
Modified Shockley–Reed–Hall model
Impurity photovoltaic effect

ABSTRACT

Silicon photodiodes have proved to be excellent detectors in the visible wave length range. On the other hand, high-performance photodetectors development remains needed. This research paper will focus on the calculation and improvement of photogenerated current of PN silicon photodetectors enhanced by the impurity photovoltaic effect. Various parameters that affect the behavior of the photogenerated current will be analyzed and studied using simulation techniques, namely MATLAB. Other aspects for the improvement of the device will include the responsiveness and the extension of the operating wavelength range. Different types and densities of impurities will be considered, analyzed and discussed. Four metallic impurities are used in the simulation, which are namely boron, indium, gallium, and aluminum. On the issue of validation of the data obtained from in this paper a practical investigation was conducted in a separate research work which involved laboratory preparation of silicon samples with indium or aluminum. Only one figure out of many will be presented in this paper. It will be seen that the variation of the photogenerated current with wavelength has a similar profile, which indicates the good agreement of the results

Contents

1. Introduction

Silicon photonics development and progress can be considered as the most dynamic in the field of integrated optics, with a vast production of commercial products [1]. Silicon photodiodes have proved to be very effective and efficient photodetectors in the range of visible wavelengths. However, the development and production of high-performance photodetectors on silicon CMOS platforms for the telecommunication application in the visible range of wavelength remains up to date not complete. Recently, however, research literature shows that some silicon photo detectors in the near infrared range have been proposed and integrated for power monitoring and optical interconnection [2–4]. On the other hand, recent rapid progress in the technological processes for the use of silicon-on-insulator (SOI) substrates has led the way for the generation of a wide range of reliable and efficient fully CMOS-compatible optical photonics components. These components include high speed modulators, low-loss waveguide, high-Q resonators, couples and optically pumped lasers [5–10]. Silicon photodetectors with high speed resonant cavity, using reflecting silicon on insulator substrates have been reported in some

* Corresponding author. +96 2796423962.
E-mail addresses: wagahfaljubori@yahoo.com, wagah2000@yahoo.co.uk (W.F. Mohammed), pureman@yahoo.com (M.A. Humoody), munther_baker44@yahoo.co.uk (M.N. Al-Tikriti).

1364-0321/$ - see front matter © 2013 Elsevier Ltd. All rights reserved.
http://dx.doi.org/10.1016/j.rser.2013.05.067

research works [11]. These detectors seem to have 40% quantum efficiency and a surface with 90%refelction at 860 nm and response time of 29 ps. Bulk photodetectors can be classified as the oldest and most thoroughly understood generation of silicon optoelectronic components. They are now commercial products with operating range of wavelength below 1100 nm with the occurrence of band-to-band absorption. However, due to its transparency silicon is not considered a suitable material for photodiodes incorporated in photonics circuits operating with wavelength exceeding 1100 nm. In order to capitalize on the low cost of standards Si-CMOS processing technology numerous photodetectors have been suggested and developed employing different physical effects. These effects include, mid-band gap absorption (MBA) [12], surface-state absorption (SSA) [13], internal photoemission absorption (IPA) and two-photon absorption (TPA) [14]. It is very common that semiconductors suffer from extrinsic and intrinsic defects. The extrinsic defect is associated with foreign atoms from impurities. Intrinsic defects on the other hand are due to crystalline defects. Impurities, in many cases, are intentionally introduced as dopant or recombination centers so as to enhance the fabrication of semiconductor as devices. Unintentional defects are introduced during the phase of crystal growth or device fabrication. Defects can be classified into two categories, shallow impurities and deep centers. Shallow impurities are characterized by levels with binding energies much smaller than that of the energy gap of the hosting semiconductors. The category of deep centers defects are characterized by electronic level located near the middle of the band gap. Defects termed generation–recombination centers are deep in the band gap. These defects become recombination centers when the semiconductor has carrier density lower than its equilibrium value. It must be noted that in the case of single crystal semiconductors, deep level impurities are commonly generated by metallic impurities.

The inability of the silicon photodetector absorbing photons possessing energies less than the band gap (E_g) and the recombination life time (s) of the photogenerated carriers, limit the detector efficiency. However, deliberate inclusion of impurity atoms or defects creates energy states within the band gap which helps a significant portion of sub-band gap photons to be absorbed. This mechanism is known as the impurity photovoltaic (IPV) effect, which can be considered as a promising approach for the improvement of photodetector efficiency [15,16]. The energy states within the band gap behave as additional recombination centers, which, unfortunately, severely lower the carrier life time. On the whole, non-mid gap and deep level impurity atoms are more suitable as they create some balance between the lifetime decay and the access to the sub band gap photons. Utilizing this concept, indium (In) can be suggested for the IPV effect as it can generate energy levels at around 157 meV above the Si valence band [15]. A significant improvement in short circuit current, up to 5 mA/cm^2, can be achieved when using a modified Shockley–Reed–Hall recombination model [17]. The assumption with the use of the model is infinite mobility and the concentration of indium is sufficiently high, around 10^{17}/cm^3 so as to compensate the n-type base [15]. The validation of the simplified Shockley–Reed–Hall statistics used for modeling carrier life time in crystalline silicon has been thoroughly investigated [18]. The smallest number of recombination center density that ensures that the simplified SRH model remains accurate is determined. This enables the lifetime-based stroboscopic techniques to safely be used to determine the number. Improving the efficiency of photodetectors is investigated through combined impact of impurity photovoltaic effect and compensation [19]. The IPV effect is produced by a deep level impurity, while shallow level impurity is employed to achieve the compensation. It must be noted that the deep level impurity must be kept moderate by comparison to primary dopant in order to prevent any deterioration in the carries lifetime. Overall efficiency enhancement of photodetectors can be achieved by the improvement of the carrier lifetime through compensation. In this research paper, the parameters that affect the behavior of the photogenerated current will be analyzed and studied using simulation techniques. The simulation will be focus on the calculation and improvement of photogenerated current of PN silicon photodetector enhanced by impurity photovoltaic effect. The improvement of the device will be mainly, concentrated on the device responsivity and the extension of the range of the operating wave length. Different types and densities of impurity will be considered, analyzed and discussed. Four metallic impurities are used in the simulation, which are namely boron (B), indium (In), gallium (Ga) and aluminum (Al).

2. Modified Shockley–Read–Hall model

In a standard Shockley–Read–Hall (SRH) model [20], electrons and holes be captured by impurity level and thermally excited from the impurity level. The six impurities related transition included in the modified SRH model is shown in Fig. 1. Under steady state condition the impurity level occupancy does not change with time, so that the net rate for electron capture (E_{cap}) by the impurity is balanced by the net rate of holes capture (H_{cap}). The net recombination rate via an impurity level can be expressed as [21]

$$U(x) = \frac{np - n_1^* p_1^*}{\tau_{no}[p + p_1^*] + \tau_{po}[n + n_1^*]}, \tag{1}$$

where n and p are the electrons and holes concentrations and τ_{no} and τ_{po} are SRH low injection lifetimes for electrons and holes and they can be expressed as follows:

$$\left.\begin{aligned} \tau_{no} &= 1/C_n N_t \\ \tau_{po} &= 1/C_p N_t \end{aligned}\right\} \tag{2}$$

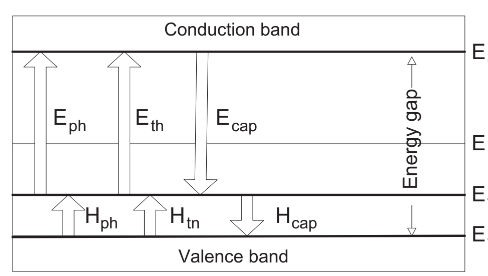


Fig. 1. Modified Shockley–Read–Hall (SRH) transitions model.

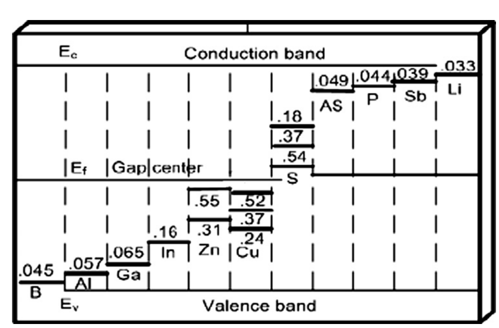


Fig. 2. Energy levels of some impurities appear at the energy gap of silicon material.

$$\left.\begin{array}{l} n_1^* = n_1 + \tau_{no} g_{n\max} \\ p_1^* = p_1 + \tau_{po} g_{p\max} \end{array}\right\}, \tag{3}$$

where n_1 and p_1 are the impurity electrons and holes concentrations and N_t is the impurity concentration. C_n and C_p are the electrons and holes capture coefficients and $g_{n\max}$ is the optical emission rate of electrons from the impurity level which is fully occupied. $g_{p\max}$ is the optical emission rate of holes from the impurity level which is completely empty. The basic idea of Eq. (1) is that for some impurities incorporated into a photodetectors, the recombination rate (U) may be positive or negative.

As far as SRH recombination mechanism is concerned, the impurity acts either to increase recombination, i.e., U is positive, that lead to decrease the carrier life time, consequently decreasing current generation, or to increase current generation in the device when U is negative. In order to increase the current generation by making U negative, this requires

$$np - n_1^* p_1^* < 0. \tag{4}$$

So, $n_1^* p_1^*$ must be as large as possible. Using Eq. (3), Eq. (4) can be rewritten as

$$np - (n_1 + \tau_{no} g_{n\max}) \times (p_1 + \tau_{po} g_{p\max}) < 0 \tag{5}$$

For midgap impurity levels $n_1 \cong p_1 \cong n_i$, therefore placing strong requirements on both photoemission terms in Eq. (5).

If impurities are added to the semiconductor material, some new energy levels will appear inside the energy gap, as shown in Fig. 2 [20]. These new energy levels will be distributed throughout the energy gap depending on the type of impurity. Some impurities produce more than one energy level. Adding such impurities will extend the range of absorbed wavelengths by producing sub energy gaps inside the original energy gap. Photons of energy less than the energy band will be absorbed by these sub energy gaps. Electron–hole pair generation occurs in two stages, as shown in Fig. 1. One of these two stages determines the rate and type of generation. The location of energy level and the stage of generation must be taken in account when the impurity is chosen.

A shallow impurity level gives rise to an asymmetry between n_1 and p_1. For the case at hand of shallow acceptor $p_1 \gg n_1$, which means that only one of the photo excitation process is crucial for $n_1^* p_1^*$ to be large, i.e., $\tau_{no} g_{n\max}$ should be large. The smallness of n_1 indicates that the electron photoemission term $g_{n\max}$ is crucial for the recombination rate to be negative, thus

$$n_1^* p_1^* \cong p_1 \tau_{no} g_{n\max}. \tag{6}$$

$g_{n\max}$ and $g_{p\max}$ can be expressed in terms of cross sections of optical emission ($\sigma_{\rm opt}$) and photon flux density ($\varphi_{\rm ph}$) as follows:

$$g_{n\max} = N_t \int_{\lambda_{\min}}^{\lambda_{\max}} \sigma_{n\rm opt}\, \varphi_{\rm ph}(x, \lambda)\, d\lambda \tag{7}$$

$$g_{p\max} = N_t \int_{\lambda_{\min}}^{\lambda_{\max}} \sigma_{p\rm opt}\, \varphi_{\rm ph}(x, \lambda)\, d\lambda, \tag{8}$$

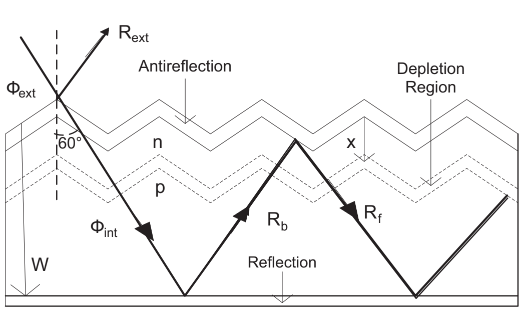


Fig. 3. Lambertian model to enhance light trapping.

where $\sigma_{n\rm opt}$ and $\sigma_{p\rm opt}$ are the cross sections of optical emission for electrons and holes respectively.

The Lambertian model shown in Fig. 3 is used to explain the light trapping in the device [18].

It is suggested that the surface is formed from inverted pyramids to disperse the light all over the detector body. Also, the device is coated with antireflection material at the front layer and reflection material at the rear layer. The angle of incident is 60° with the vertical to the device surface. The general expression of photon flux density at distant x from the surface is

$$\Phi_{\rm ph}(x, \lambda) = (1 - R_{\rm ext}(\lambda)) \frac{1 + e^{-4(w-x)\alpha_t} R_b}{1 - e^{-4w\alpha_t} R_b R_f} \times e^{-2x\alpha_t} \Phi_{\rm ext}(\lambda), \tag{9}$$

where α_t is the total absorbance coefficient, $R_{\rm ext}$ is the external reflectance at front layer, R_f is the internal reflectance at front layer and R_b is the internal reflectance at the rear layer. For typical working device of no external reflectance ($R_{\rm ext}=0$) and full internal reflectance ($R_b=1$), knowing that $R_f=1-1/N^2$, N is the refractive index of silicon which is equal to 3.45. Eq. (9) will be reduced to $\varphi_{\rm ph}(\lambda)=2N^2\varphi_{\rm ext}(\lambda) \cong 25\varphi_{\rm ext}(\lambda)$. That means the internal photon flux is enhanced by the factor 25.

2.1. Photogenerated current simulation

The photogenerated current density ($J_{\rm ph}$) inside the device due to impurity doping is given by [22]

$$J_{\rm ph} = q \int_o^{xj} [-U(x)]\, dx, \tag{10}$$

where q is the electronic charge and x_j is the junction depth.

Substituting Eq. (1) in Eq. (10) yields

$$J_{\rm ph} = -q \int_o^{x_j} \frac{np - n_1^* p_1^*}{\tau_{no}(p + p_1^*) + \tau_{po}(n + n_1^*)}\, dx \tag{11}$$

Substituting τ_{no}, τ_{po}, n_1^* and p_1^* from Eqs. (2), (3), (7) and (8) in Eq. (11) and knowing that

$$n_1 = g_t N_c e^{-(E_c - E_t/)kT} \text{ and } p_1 = \frac{1}{g_t} N_v e^{-(E_t - E_v/kT)} \tag{12}$$

where g_t is the impurity level degeneracy, N_c and N_v are the effective density of states in the conduction and valence bands respectively, E_c and E_v are the conduction and valence band edges, E_t is the effective impurity level, k is the Boltzmann constant and T the temperature in Kelvin (see Eq. (13) below).

Knowing the values of g_t, N_c, N_v, n, p, C_n, C_p, σ_n, σ_p and $x_j=0.3$ μm, Eq. (13) can be solved numerically using the MATLAB program and the values of the photogenerated current can be calculated. The photogenerated current depends on the photon flux density, which is a function of spectrum wavelength, impurity concentration, and its depth inside the device and the device reflectivity.

3. Results and discussions

All relevant parameters of the elements, which have been used in the study and soluble in silicon material, are summarized in Table 1 [21, 23–26]. Different types of impurities with different concentrations were used to investigate the effect of these parameters on the performance and behaviors of photodetectors. The investigations were carried out on samples doped with impurity around 0.3 μm deep from the surface using simulation techniques, mainly MATLAB Programs.

The variations of photogenerated current with respect to wavelength of boron doped samples without front antireflection and without rear reflection are shown in Fig. 4. It can be deduced

Table 1
Impurities parameters soluble in silicon material.

Impurity parameter	In	Ga	Al	B	Reference
Energy level E_t (eV)	E_v+0.16	E_v+0. 67	E_v+0.57	E_v+0.54	[23]
Degeneracy g_t	4	4	4	4	[24]
Holes density p_1 (cm^{-3})	1.6×10^{16}	6.3×10^{17}	8.58×10^{17}	1.36×10^{18}	[21]
Electrons density n_1 (cm^{-3})	9.14×10^{3}	2.33×10^{2}	1.71×10^{2}	1.1×10^{2}	[21]
Hole capture coefficient C_p (cm s^{-1})	8×10^{-8}	6.67×10^{-7}	2×10^{-7}	1.11×10^{-7}	[24]
Electron capture coefficient C_n (cm s^{-1})	2×10^{-15}	1×10^{-15}	1×10^{-16}	8.3×10^{-17}	[25]
Hole optical emission σ_{nopt} (cm^2)	0.5×10^{-16}	2.6×10^{-16}	8×10^{-16}	14×10^{-16}	[24, 25]
Electron optical emission σ_{popt} (cm^2)	9×10^{-18}	10×10^{-19}	5.3×10^{-19}	3.19×10^{-19}	[26]
Solubility (cm^{-3})	1×10^{18}	4×10^{19}	2×10^{19}	6×10^{20}	[26]

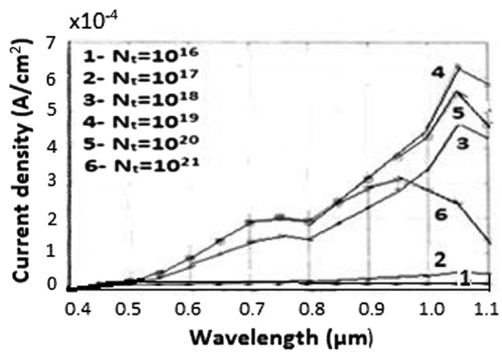


Fig. 4. Variation of photogenerated current with wavelength of boron doped sample without front antireflection and rear reflection.

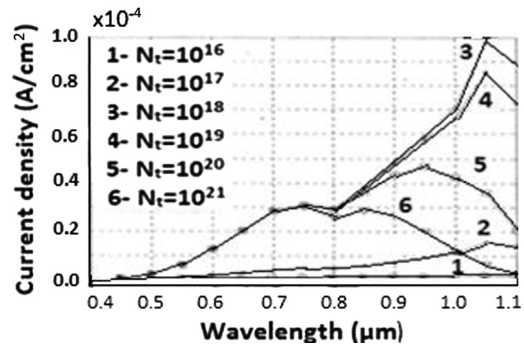


Fig. 6. Variation of photogenerated current with wavelength of gallium doped sample without front antireflection and rear reflection.

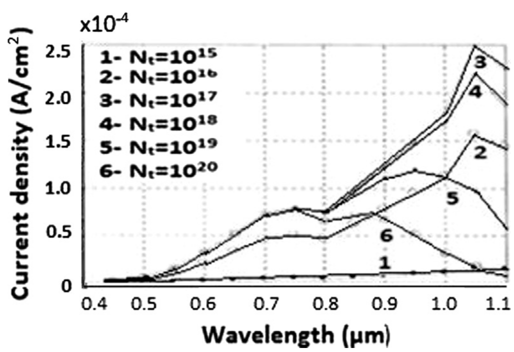


Fig. 5. Variation of photogenerated current with wavelength of indium doped sample without front antireflection and rear reflection.

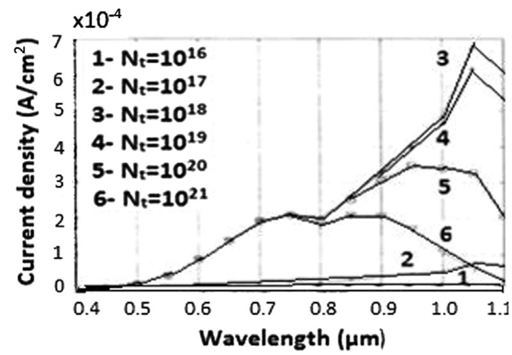


Fig. 7. Variation of photogenerated current with wavelength of aluminum doped sample without front antireflection and rear reflection.

that increasing the impurity concentration improves the photogenerated current and also widen the operating wavelength range toward near infrared region. More specifically the current starts to rise when the concentration of the impurities exceeds the value 10^{16}/cm^3 and exhibit peak value at $N_t = 10^{19}$/cm^3 when the concentration of the impurities almost equal to the electron concentration of the primary dopant in the window layer. Beyond this value of concentration, the photogenerated current tends to decline in value.

$$J_{ph} = -q \int_0^{xj} \frac{np - [n_1 + (1/C_n N_t)\{N_t \int_{\lambda_{min}}^{\lambda_{max}} 2\sigma_{nopt}(\lambda)\Phi_{ph}(x,\lambda)\, d\lambda\}][p_1 + (1/C_p N_t)\{N_t \int_{\lambda_{min}}^{\lambda_{max}} 2\sigma_{popt}(\lambda)\Phi_{ph}(x,\lambda)\, d\lambda\}]}{1/C_n N_t[p + p_{1+}(1/C_p N_t)\{N_t \int_{\lambda_{min}}^{\lambda_{max}} 2\sigma_{popt}(\lambda)\Phi_{ph}(x,\lambda)\, d\lambda\}] + (1/C_n N_t)\{n + n_1 + (1/C_p N_t)\{N_t \int_{\lambda_{min}}^{\lambda_{max}} 2\sigma_{nopt}(\lambda)\Phi_{ph}(x,\lambda)\, d\lambda\}\}} dx \quad (13)$$

The explanation for this is the decrease of carrier lifetime. On the whole, carrier lifetime is inversely proportional with the concentration of the carrier, according to Eqs. (2) and (3). U will be positive when the values of n_1^* and p_1^* decrease, this consequently indicates that the process at hand is a recombination process rather than a generation process. The sample exhibited peak responsivity at 1.05 μm wavelength, but it decreases to 0.4–0.7 μm at lower and higher impurity concentrations.

Figs. 5–7 display the variation of the photogenerated current with respect to wavelength without front antireflection and without rear reflection for different impurity concentrations of In, Ga and Al. On the whole, it can be noted that the responsivity will exhibit peak values at around 1.05 μm for all samples. Indium doped samples had the highest photogenerated current at

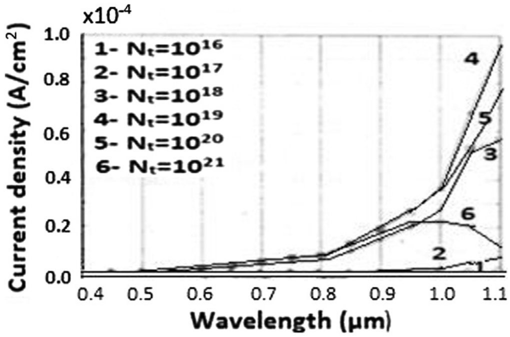


Fig. 8. Variation of photogenerated current with wavelength of boron doped sample with full front antireflection and rear reflection.

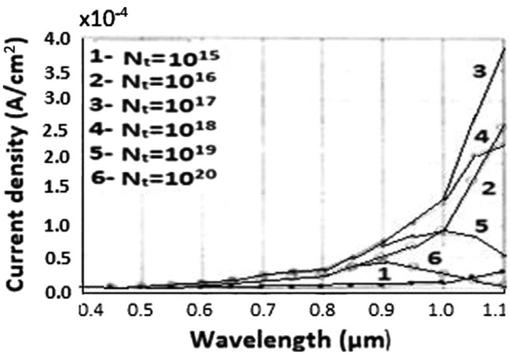


Fig. 9. Variation of photogenerated current with wavelength of indium doped sample with full front antireflection and rear reflection.

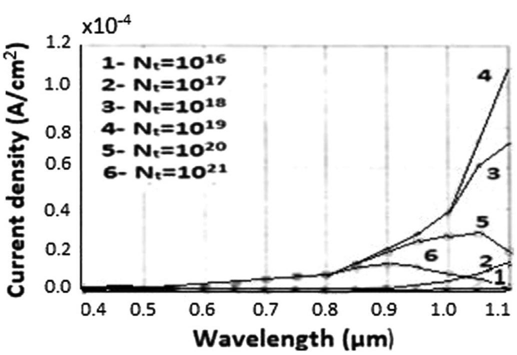


Fig. 10. Variation of photogenerated current with wavelength of gallium doped sample with full front antireflection and rear reflection.

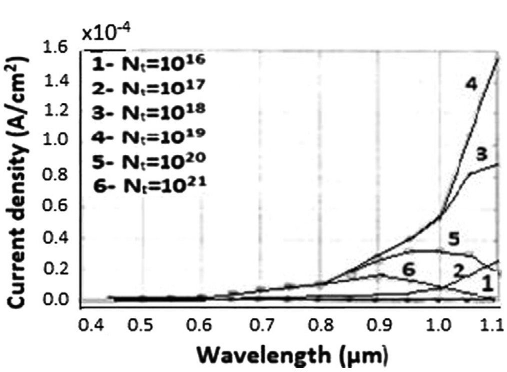


Fig. 11. Variation of photogenerated current with wavelength of aluminum doped sample with full front antireflection and rear reflection.

10^{17}/cm^3 impurity concentration [27,28]. Gallium and alumium doped samples had the highest photogenerated current at 10^{18}/cm^3 impurity concentration. All these results are in

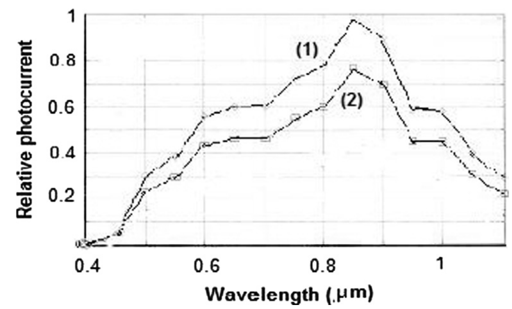


Fig. 12. Variation of photogenerated current of the laboratory prepared samples: (1) indium and (2) aluminum, with wavelength at −3 V reverse voltage.

agreement with what was reported by Sclar [29]. It can be concluded that the value of the photogenerated current is varied with the varation of impurity type and its concentration. The varation of peak value of photogenerated current with regard to the impurity concentration is attributed to the difference of impurity solubility as stated in Table 1. Boron has the highest solubilityof 6×10^{20}/cm^3, while indium has the lowest at 10^{18}/cm^3. Impurity with the lowest solubility tends to have highest cross section optical emission (σ_{nop}) which pushes the rate of generation ($g_{n\max}$) up, as can be deduced from Eqs. (7) and (8). This will lead to the increase of the photogenerated current [26]. It is abvious now that the solubility of the impurities limits the employment of high impurity concentration in photodetectors. Indium concentration beyond 10^{18}/cm^3 causes the photogenerated current to decline, while the current declines for gallium and aluminum at concentration 10^{19}/cm^3 and at 10^{20}/cm^3 for boron impurities.

The varaition of the simulated photogenerated current versus the wavelength with antireflection layer at the front and reflection layer at the rear are taken into account are shown in Figs. 8–11. It is clearly evident that the photogenerated current has increased by almost ten-fold for all samples. The reason for this is related to the enhancementof the internal photo flux density at the expense of the external density. It is very interesting to note the extention of the oprating wavelength range to 1.1 μm at which the photogenerated current reaches the peak. This may support the idea of using some kind of light concentrator to push the detection range of silicon photodetectors far into infrared.

The photoelectronic properties of practically fabricated silicon photodetector doped with indium or aluminum were investigated and compared with simulated results. It can be deduced that high photogenerated current were produced by silicon samples doped with indium of thickness 1500 Å or aluminum of thickness 2000 Å. These thicknesses correspond to around 10^{17}/cm^3 for indium and around 10^{18}/cm^3 for aluminum.

Fig. 12 shows the variation of photogenerated current of the laboratory prepared samples with wavelength at −3 V reverse voltage. In general the profiles of the curves are the same as that produced by the simulation. It can be noted that the photogenerated current for aluminum samples is less than that for indium samples despite the fact that the impurity concentration of aluminum is higher. This can be explained as result of the fact that optical emission cross section of indium is higher than that for aluminum.

4. Conclusion

Research in the development of high-performance photodetectors with sufficient photogenerated current and wide visible wavelength suitable for such applications as optical interconnection and power monitoring is of great interest nowadays.

Simulation techniques are powerful and useful approaches to study the enhancement of the performance of PN silicon photodetectors. The results obtained indicate that increasing the impurity concentration improves the photogenerated current and moreover widen the operating wavelength range toward near infrared region. The increase in the current exhibits peak value that depends on the level of impurity concentration and the type of impurity used. However, it can be deduced that, on the whole and for all four types of impurities, the responsivity of the device reaches peak values at 1.05 μm wavelength. Indium doped samples produced the highest photogenerated current with the lowest impurity concentration of $10^{17}/cm^3$ as compared with boron, gallium and aluminum. These simulated results are for samples without front antireflection and without rear reflection. On the other hand simulated photogenerated currents versus the wavelength for samples with antireflection layer at the front and reflection layer at the rear shows that the photogenerated current can be increased by almost ten folds for all samples. This is due to the enhancement of the internal photo flux density at the expanse of the external density.

Acknowledgment

The authors are deeply grateful to Mosul University for their technical support. They are grateful to Suzanne Al-Tikriti for partially typing the manuscript.

References

[1] Casalino M, Coppola G, Iodice M, Rendina I, Sirleto L. Near-infrared sub-bandgap all-silicon photodetectors: state of the art and perspectives. Sensors 2010;10:10571–600, http://dx.doi.org/10.3390/s101210571.
[2] Mohammad WF, Abouhajar A, Saleh AN. Effect of oxide layers and metals on photoelectric and optical properties of Schottky barrier photo detector. Renewable Energy Journal, England 2006;31(10):1493–503.
[3] Mohammad WF, Khatib NN. Investigations of current mechanisms and electronic properties of Schottky barrier diode. Manager's Journal on Electronics Engineering 2012;2l(3l):30–6.
[4] Mohammed, WF, Al-Tikriti, MN, Khatib, NN. Fabrication and investigation of MOS modified Schottky barrier photodetector. In: Proceedings of the 6th International Conference on Sensing Technology (ICST2012), 2012, Kolkata, India.
[5] Rowe LK, Elsey M, Tarr NG, Knights AP, Post E. CMOS-compatible optical rib waveguides defined by local oxidation of silicon. Electronics Letters 2007;43:392–3.
[6] Vivien L, Pascal D, Lardenois S, Marris-Morini D, Cassan E, Grillot F, Laval S, Fedeli JM, El Melhaoui L. Light injection in SOI microwave guides using high-efficiency grating couplers. Journal of Lightwave Technology 2006;24:3810–5.
[7] Xu Q, Manipatruni S, Schmidt B, Shakya J, Lipson M. 12.5 Gbit/s carrier-injection-based silicon micro-ring silicon modulators. Optics Express 2007;15:430–6.
[8] Michael CP, Borselli M, Johnson TJ, Chrystal C, Painter O. An optical fiber-taper probe for wafer-scale microphotonic device characterization. Optics Express 2007;15:4745–52.
[9] Liu A, Liao L, Rubin D, Nguyen H, Ciftcioglu B, Chetrit Y, Izhaky N, Paniccia M. High-speed optical modulation based on carrier depletion in a silicon waveguide. Optics Express 2007;15:660–8.
[10] Liu A, Jones R, Cohen O, Hak D, Paniccia M. Optical amplification and lasing by stimulated Raman scattering in silicon waveguides. Journal of Lightwave Technology 2006;24:1440–5.
[11] Emsley MK, Dosunmu O, Unlu MS. High speed resonant cavity enhanced silicon photodetectors on reflecting silicon on isolator substrate. IEEE Photonics Technology Letters 2002;14(4):516–21.
[12] Libertino S, Coffa S, Benton JL, Halliburton K, Eaglesham DJ. Formation, evolution and annihilation of interstitial clusters in ion implanted Si. Nuclear Instruments and Methods in Physics Research Section B 2001;148:247–51.
[13] Schroder DK. Semiconductor material and device characterization. New York, NY, USA: John Wiley & Sons; 2006.
[14] Casalino M, Sirleto L, Moretti L, Rendina IA. Silicon compatible resonant cavity enhanced photodetector working at 1.55 μm. Semiconductor Science and Technology 2008;23:075001.
[15] Keevers MJ, Green MA. Efficiency improvement of silicon solar cells by impurity photovoltaic effect. Journal of Applied Physics 1994;75:4022–31.
[16] Macdonald D, Mc Lean K, Deenapanray PNK, DeWolf S, Schmidt J. Electronically-coupled up-conversion: an alternative approach to impurity photovoltaic in crystalline silicon. Semiconductor Science and Technology 2008;23:015001.
[17] Shockley W, Read WT. Statistics of the recombination's of holes and electrons. Physical Review 1952;87(5):835–42.
[18] Macdonald D, Cuevas A. Validity of simplified Shockley–Read–Hall statistics for modeling carrier lifetimes in crystalline silicon. Physical Review 2003;B 67 (No. 7):5203–10.
[19] Pavel AA, Rezwan Khan M, Islam NE. On the possibility of improving silicon solar cell efficiency through impurity photovoltaic effect and compensation. Solid-State Electronics 2010;54:1278–83.
[20] Shockley W, Queissey HJ. Detailed balance limit of efficiency of pn junction solar cells. Journal of Applied Physics 1961;33:510.
[21] Green MA, Keevers MJ. Optical properties of intrinsic silicon at 300 K. Progress in Photovoltaic Research and Applications 1995;3:189–92.
[22] Mohamad WF, Khalel KH. Infrared response and quantum efficiency of In-doped silicon (n) structure. Renewable Energy Journal 2000;3-4:1.
[23] Willardson RK, Beer AC. Semiconductors and semimetals: hydrogenated amorphous silicon", Part D: device applications (semiconductors and semimetals). Academic Press; 978-0-12-752112-1.
[24] Sclar N. Asymmetries in photoconductive properties of donor and acceptor impurities in silicon. Journal of Applied Physics 1984;55:2972.
[25] Geim K, Pensl G, Schulz M. Shallow accepter population and free hall concentration in Si:In and Si:Ge with IR photo excitation. Applied Physics A: Materials Science and Processing 1982;27(2):71–8, http://dx.doi.org/10.1007/bf00615808.
[26] Abakumov VN, Perel VI, Yassievich IN. Capture of carriers by attractive centers in semiconductors (Review). Soviet Physics Semiconductors 1978;12(1):1–18.
[27] Hobgood HM, Braggins TT, Sopira MM, Swartz JC, Thomas RN. Growth and characterization of Indium-doped silicon for extrinsic IR detectors. IEEE Transactions on Electron Devices 1980;27(1):14–23.
[28] Braggins TT, Hobgood HM, Swartz JC, Thomas RN. High infrared responsitivity Indium-doped silicon detector material compensated by neutron transmutation. IEEE Transactions on Electron Devices 1980;27(1):2–10.
[29] Sclar N. Extrinsic silicon detectors for 3–5 and 8–14 μm. Infrared Physics 1976;16(4):435–48.